GEOPHYSICS

# Slow slip source characterized by lithological and geometric heterogeneity

Philip M. Barnes[1]*, Laura M. Wallace[2], Demian M. Saffer[3†], Rebecca E. Bell[4], Michael B. Underwood[5], Ake Fagereng[6], Francesca Meneghini[7], Heather M. Savage[8], Hannah S. Rabinowitz[9‡], Julia K. Morgan[10], Hiroko Kitajima[11], Steffen Kutterolf[12], Yoshitaka Hashimoto[13], Christie H. Engelmann de Oliveira[14], Atsushi Noda[15], Martin P. Crundwell[2], Claire L. Shepherd[2], Adam D. Woodhouse[16], Robert N. Harris[17], Maomao Wang[18], Stuart Henrys[2], Daniel H.N. Barker[2], Katerina E. Petronotis[19], Sylvain M. Bourlange[20], Michael B. Clennell[21], Ann E. Cook[22], Brandon E. Dugan[23], Judith Elger[12], Patrick M. Fulton[24], Davide Gamboa[25], Annika Greve[26§], Shuoshuo Han[27], Andre Hüpers[28], Matt J. Ikari[28], Yoshihiro Ito[29], Gil Young Kim[30], Hiroaki Koge[31], Hikweon Lee[30], Xuesen Li[32], Min Luo[33], Pierre R. Malie[34], Gregory F. Moore[35], Joshu J. Mountjoy[1], David D. McNamara[36], Matteo Paganoni[37‖], Elizabeth J. Screaton[38], Uma Shankar[39], Srisharan Shreedharan[3], Evan A. Solomon[40], Xiujuan Wang[41], Hung-Yu Wu[26¶], Ingo A. Pecher[42], Leah J. LeVay[19]; IODP Expedition 372 Scientists[43]



**Slow slip events (SSEs) accommodate a significant proportion of tectonic plate motion at subduction zones, yet little is known about the faults that actually host them. The shallow depth (<2 km) of well-documented SSEs at the Hikurangi subduction zone offshore New Zealand offers a unique opportunity to link geophysical imaging of the subduction zone with direct access to incoming material that represents the megathrust fault rocks hosting slow slip. Two recent International Ocean Discovery Program Expeditions sampled this incoming material before it is entrained immediately down-dip along the shallow plate interface. Drilling results, tied to regional seismic reflection images, reveal heterogeneous lithologies with highly variable physical properties entering the SSE source region. These observations suggest that SSEs and associated slow earthquake phenomena are promoted by lithological, mechanical, and frictional heterogeneity within the fault zone, enhanced by geometric complexity associated with subduction of rough crust.**

## INTRODUCTION

The physical processes that underlie episodic slow slip events (SSEs) are widely debated, but widely held hypotheses invoke a combination of transitional frictional properties of fault rocks and elevated pore pressure, which reduces the effective normal stress (*1*–*3*). These hypotheses are rooted in interpretations of geophysical survey data, tidal modulation of tremor and SSE, numerical modeling, and laboratory measurements of frictional properties for both natural fault rocks and synthetic analogs (*1*–*7*). Frictional, rheological, and geometrical heterogeneity within fault zones has also emerged as a possible key ingredient in promoting SSEs (*2*, *3*, *8*–*11*). Testing these ideas requires direct observations of physical conditions and rock compositions within SSE source regions.

The northern Hikurangi subduction zone offshore New Zealand hosts some of the most intensively studied shallow SSEs on Earth. Here, the Pacific Plate subducts westward beneath the North Island at a rate of ~5 cm/year (*12*). The subducting crust is composed of the Hikurangi Plateau, a Cretaceous large igneous province (*13*, *14*). The incoming plateau is blanketed in most places by ~1 to 1.5 km of sediment and is studded with basaltic seamounts that protrude through the sedimentary cover (Fig. 1). Subduction of seamounts along the margin has resulted in complex deformation and erosion of the frontal accretionary wedge (*15*–*17*). Shallow (<15 km depth) SSEs recorded by continuous GPS measurements recur every 1 to 2 years (*18*). Seafloor geodetic data suggest that the SSEs propagate to within 2 km of the seafloor and possibly all the way to the trench (*19*). Tremor and microseismicity are observed within and surrounding the SSE source, and are locally associated with seamount subduction (*20*–*22*). The shallow megathrust probably hosted two $M_w$ (moment magnitude) 7.0 to 7.2 earthquakes in 1947, which generated 8- to 10-m tsunami along the coast (*23*, *24*). These observations indicate that the very shallow plate boundary megathrust may host both large earthquakes and aseismic slow slip.

The close proximity of slow slip to the seafloor at north Hikurangi has attracted a wide range of investigations focused on the mechanics and processes that underlie slow earthquake phenomena. As part of these efforts, International Ocean Discovery Program (IODP) Expeditions 372 and 375 logged, cored, and installed observatories along a transect spanning the shallow SSE source region, from the subducting plate to the overriding plate (Fig. 1) (*25*). Here, we combine drilling results from two sites on the incoming plate with regional seismic reflection profiles to track the sedimentary sequence on the subducting plate into the SSE source region along the plate interface (Figs. 1 and 2). Although drilling directly sampled the incoming plate seaward of the actual plate interface, it accessed the materials entrained along and beneath the megathrust. In combination with interpretations of regional seismic reflection data, this provides insight into the composition, geometry, and physical properties of a plate boundary fault that hosts well-documented, large SSEs.

## RESULTS

### Tracking materials from the subducting plate into the SSE source zone

The plate interface along the drilling transect is characterized by coherent seismic reflections beneath the outer ~15 to 20 km of the frontal accretionary wedge [common depth point (CDP), 3500 to 4400] ~5 to 6 km below sea level (Fig. 2). Beneath the mid-slope (CDP, 2600 to 2900), the interface exhibits weak seismic reflectivity where it overlies an inferred subducted seamount (*5*, *21*). Further

down-dip (Fig. 1; CDP, 1000 to 2300), the interface overlies a low-velocity, highly reflective zone (HRZ), previously interpreted to comprise fluid-rich subducted sediments (*5*, *21*). Beneath the Hikurangi Trough seaward of the plate boundary, the sedimentary cover sequence includes an upper succession with weaker, continuous seismic reflectivity and a more reflective lower succession (Fig. 2 and fig. S1). This cover sequence overlies the plateau basement units HKB (Hikurangi Basement) and VB (Volcanic Basement), which are characterized by discontinuous high-amplitude seismic reflections and interpreted as Upper Cretaceous [<120 million years (Ma) old] volcanic and volcaniclastic sequences (*13*).

Our mapping of the basement surface (the top of units HKB and VB) in seismic data for >100 km along strike highlights substantial relief (>2 km) and roughness on the incoming basement at scales ranging from <1 km to tens of kilometers (Fig. 3). Some areas of positive relief are completely buried beneath the sedimentary cover sequence. Others, including the Tūranganui Knoll seamount, protrude above the basin floor and support smaller-scale volcanic cones on their crest up to ~400 m in height (Fig. 2B). Along the drilling transect, we correlate the stratigraphic interval that hosts the plate interface with the lower sedimentary succession and the upper levels of units HKB and VB (blue shading in Fig. 2). On the subducting oceanic plate, this interval is geometrically complex in three dimensions (Fig. 3).

## Lithologies and physical properties of the slow slip protolith rocks

Two sites on the subducting Pacific Plate were drilled to acquire core samples and geophysical logs and to measure the physical properties of material being transported into the SSE source region (see the Supplementary Materials) (*25*). Site U1520 is located east (seaward) of the deformation front in the Hikurangi Trough (Figs. 1 and 2B). Site U1526 is atop the Tūranganui Knoll seamount. At Site U1520, we cored to 1054 m below seafloor (mbsf) and acquired logging-while-drilling (LWD) data and wireline logs to 947 mbsf (figs. S2 and S3). We tied the core and logging data to seismic profile 05CM-04 using a synthetic seismic trace constructed from drilling data (*25*) and then correlated the sequences away from the drilling site to the plate boundary (Fig. 2 and fig. S2). Coring of this interval recovered an uppermost section of mainly Pleistocene siliciclastic trench sediments (to ~510 mbsf) and a sequence of predominantly pelagic carbonates and volcaniclastics below.

On the basis of our regional seismic correlations (Fig. 2), the key protolith interval, in which the subduction plate interface most likely forms and eventually hosts SSEs, lies below 650 mbsf at Site U1520 (Fig. 4A and fig. S3). The upper part of this interval includes marl-dominated (calcareous mudstone) and chalk-dominated pelagic rocks (650 to 849 mbsf) of Paleocene to Miocene (66 to 9 million years old) age (e.g., Lithologic unit IV, core photographs 1 to 4; Fig. 4A) (*25*). These rocks have porosities of ~30 to 48%, *P*-wave velocities increasing with depth from ~2.1 to 2.7 km/s, and contain cements and alteration products indicative of early diagenesis. This part of the sediment section includes alternating clay-rich (dominantly smectite) and carbonate-rich zones a few centimeters to several tens of meters thick (Fig. 4A and fig. S3).

Beneath the pelagic section, we sampled ~170 m of variably cemented and intensely altered Upper Cretaceous volcaniclastic conglomerate (e.g., Lithologic unit V, core photograph 4; Fig. 4A), with a minor interval of marl (calcareous mudstone). The vast majority of clasts throughout the volcaniclastic conglomerate are well rounded,

[1]National Institute of Water and Atmospheric Research (NIWA), Wellington 6021, New Zealand. [2]GNS Science, Lower Hutt 5011, New Zealand. [3]Department of Geosciences and Center for Geomechanics, Geofluids, and Geohazards, The Pennsylvania State University, University Park, PA 16802, USA. [4]Basins Research Group, Imperial College London, Exhibition Road, Kensington SW7 2AZ, UK. [5]Department of Earth and Environmental Science, New Mexico Institute of Mining and Technology, 801 Leroy Place, Socorro, NM 87801, USA. [6]School of Earth and Ocean Sciences, Cardiff University, Park Place, Cardiff CF10 3AT, UK. [7]Dipartimento di Scienze della Terra, Università degli Studi di Pisa, via. S. Maria, 53, Pisa 56126, Italy. [8]Department of Earth and Planetary Sciences, University of California, 1156 High St., Santa Cruz, CA 95064, USA. [9]Department of Earth, Environmental, and Planetary Sciences, Brown University, 324 Brook Street, Providence, RI 02912, USA. [10]Department of Earth Science, Rice University, 6100 South Main Street, MS-126, Houston, TX 77005-1892, USA. [11]Department of Geology and Geophysics, Texas A&M University, MS 3115 TAMU, College Station, TX 77845, USA. [12]GEOMAR, Helmholtz Center for Ocean Research, Kiel, Wischhofstrasse 1-3, Kiel 24148, Germany. [13]Department of Natural Environmental Science, Faculty of Science, Kochi University, Akebonocyo 2-5-1, Kochi 780-8520, Japan. [14]Programa de Pós-Graduação em Geologia, Universidade do Vale do Rio dos Sinos, Avenida Unisinos 950, São Leopoldo RS 93.022-000, Brazil. [15]Geological Survey of Japan, National Institute of Advanced Industrial Science and Technology (AIST), Central 7, 1-1-1 Higashi, Tsukuba, Ibaraki 305-8567, Japan. [16]School of Earth and Environment, University of Leeds, Leeds LS2 9JT, UK. [17]College of Earth, Ocean and Atmospheric Sciences, Oregon State University, Ocean Administration Building, 104, 101 SW 26th Street, Corvallis, OR 97331-5503, USA. [18]College of Oceanography, Hohai University, 1 Xikang Road, Nanjing, Jiangsu Province 210093, P.R. China. [19]International Ocean Discovery Program, Texas A&M University, College Station, TX 77845, USA. [20]Ecole Nationale Superieure de Geologie—Laboratoire GeoRessources, Universite de Lorraine, 2 rue du Doyen Marcel Roubault, BP 10162, 54505 Vandoeuvre-les-Nancy Cedex, France. [21]Energy, CSIRO, 26 Dick Perry Avenue, Kensington 6151, Australia. [22]School of Earth Sciences, Ohio State University, 317 Mendenhall Lab, 125 S. Oval Mall, Columbus, OH 43202, USA. [23]Department of Geophysics, Colorado School of Mines, 1318 Maple Street, Bldg. 6, Golden, CO 80401, USA. [24]Department of Earth and Atmospheric Sciences, Cornell University, 3126 Snee Hall, Ithaca, NY 14853-1504, USA. [25]Instituto Português do Mar e da Atmosfera, I.P. (IPMA), Rua C ao Aeroporto, 1749-077 Lisboa, Portugal. [26]Institute for Marine-Earth Exploration and Engineering, Japan Agency for Marine-Earth Science and Technology, Yokosuka, Japan. [27]Institute for Geophysics, University of Texas, 10100 Burnet Road, Austin, TX 78758, USA. [28]MARUM Center for Marine Environmental Sciences and Faculty of Geosciences, University of Bremen, Leobener Strasse 8, Bremen 28359, Germany. [29]Disaster Prevention Research Institute, Kyoto University, Gokasyo, Uji, Kyoto 611-0011, Japan. [30]Korea Institute of Geoscience and Mineral Resources (KIGAM), 124 Gwahang-no, Yuseong-gu, Daejeon 305-350, Republic of Korea. [31]Marine Geology Research Group, GSJ, AIST Central 7, 1-1-1 Higashi, Tsukuba, Ibaraki 305-8567, Japan. [32]College of Earth Science, Guilin University of Technology, 12 Jian gan Road, Guilin City 541004, P.R. China. [33]Shanghai Engineering Research Center of Hadal Science and Technology, College of Marine Sciences, Shanghai Ocean University, Shanghai 201306, P.R. China. [34]Geosciences Montpellier Laboratory, Université Montpellier, CC.60, Place E. Bataillon, 34095 Montpellier Cédex 5, France. [35]Department of Earth Sciences/SOEST, University of Hawaii at Manoa, 1680 East-West Road, Honolulu, HI 96822, USA. [36]Department of Earth, Ocean and Ecological Sciences, University of Liverpool, Jane Herdman Building, 4 Brownlow Street, Liverpool L69 3GP, UK. [37]University of Oxford, South Parks Road, Oxford OX1 3AN, UK. [38]Department of Geological Sciences, University of Florida, Gainesville, FL 32611, USA. [39]Department of Geophysics, Banaras Hindu University, Institute of Science, Varanasi Uttar Pradesh 221005, India. [40]School of Oceanography, University of Washington, Seattle, WA 98195-7940, USA. [41]Key Laboratory of Marine Geology and Environment, Chinese Academy of Sciences, Nanhai Road 7, Qingdao, Shandong 266071, P.R. China. [42]School of Environmental and Marine Sciences, University of Auckland, Private Bag 92091, Auckland 1142, New Zealand. [43]International Ocean Discovery Program, Expedition 372, Creeping Gas Hydrate Slides and Hikurangi LWD, 26 November 2017 to 4 January 2018; see the Supplementary Materials for a list of participants.
*Corresponding author. Email: philip.barnes@niwa.co.nz
†Present address: University of Texas Institute for Geophysics (UTIG), 10601 Exploration Way, Austin, TX 78758, USA.
‡Present address: Department of Energy, 955 L'Enfant Plaza SW, Washington, DC 20024, USA.
§Present address: Department of Earth Sciences, Utrecht University, Netherlands.
||Present address: Shell Global Solutions International, B.V., Rijswijk, Netherlands.
¶Present address: Department of Resources Engineering, National Cheng Kung University. No.1, University Road, Tainan City 701, Taiwan (R.O.C.).

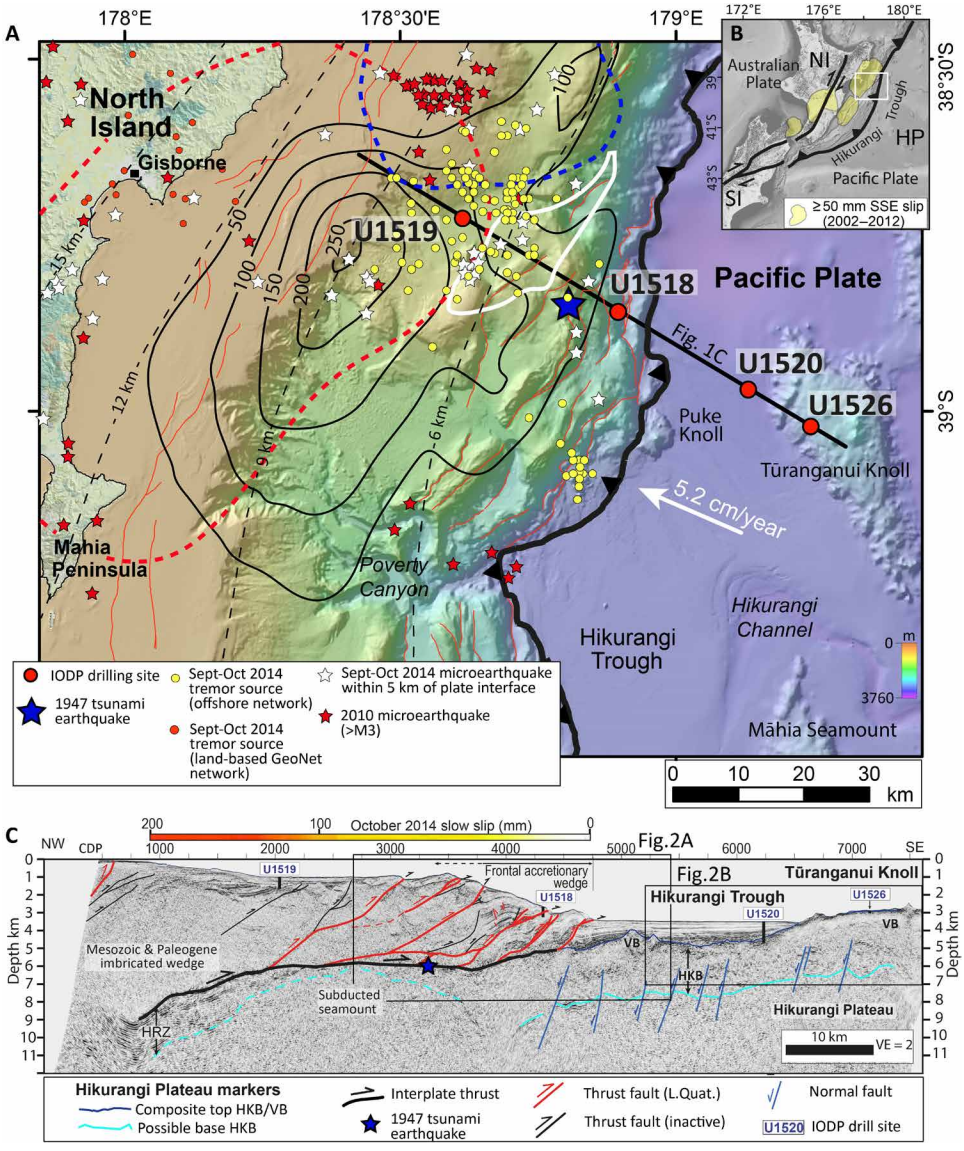


**Fig. 1. Tectonic setting of slow slip at the northern Hikurangi subduction margin.** (**A**) Bathymetric map showing the extent of three recent SSEs (*18*, *19*), associated with seismic tremor (low-frequency energy bursts in the 4- to 10-Hz frequency range) and microearthquakes (*20*, *38*). Fine black lines with labels are slip contours (mm) for the September to October 2014 SSE. Blue and red dashed lines are 40-mm slip contours for the January to February 2010 Tolaga SSE and the March to April Gisborne SSE, respectively. Dashed black lines show approximate depth to the plate interface (*39*). Bold black line with teeth marks the plate boundary deformation front. Fine red lines are upper plate thrust faults. Bold white line is the footprint (at 6.75 km depth) of an inferred subducted seamount (*21*). The 1947 tsunami earthquake location is from (*23*, *24*). PR, Puke Ridge. (**B**) Regional tectonic setting. Yellow shading shows distribution of cumulative slow slip from 2002 to 2012 (*18*). (**C**) Interpretation of seismic profile 05CM-04 [modified from (*21*, *25*)]. HRZ, highly reflective zone (*5*); HKB, Hikurangi basement; VB, volcanic basement [units adapted from (*13*)]. Colored scale shows slip in the October 2014 SSE (*19*).

basaltic, and highly altered to hydroxides, chlorite, and epidote, while the matrix is almost totally replaced by smectite, with variable cementation by zeolite and calcite. Underlying this lithologic unit, the lower part of the plate interface protolith interval is a highly mixed Upper Cretaceous assemblage of volcaniclastic conglomerate, volcaniclastic siltstone, silty claystone with minor limestone and organic-rich siltstone, and basalt (Lithologic unit VI, core photographs 5 to 8; Fig. 4A).

The mixed volcaniclastic-dominated assemblage comprising Lithologic units V and VI is characterized by highly heterogeneous physical properties and represents the upper portion of the Hikurangi Plateau (either unit HKB or VB; Figs. 1, 2, and 3C). *P*-wave velocities (~1.8 to >5.0 km/s) and porosities (~20 to 56%) vary markedly over length scales of only a few to tens of centimeters (Fig. 4A). Such large variations in physical properties primarily reflect the uneven distribution of zeolite and calcite cementation, clay alteration, and veining.

At Site U1526 atop the Tūranganui Knoll, we cored to 84 mbsf (Fig. 4B) (*25*). The upper 30 m comprises a veneer of Holocene and Pleistocene age hemipelagic mud, overlying Upper Cretaceous to Pliocene calcareous mud, and nannofossil ooze (e.g., Lithologic unit I, core photograph 1; Fig. 4B and fig. S4). Beneath this veneer, the highly reflective sequence observed in seismic data consists of coarse-grained volcaniclastic sandstone overlying alternating intervals of volcaniclastic

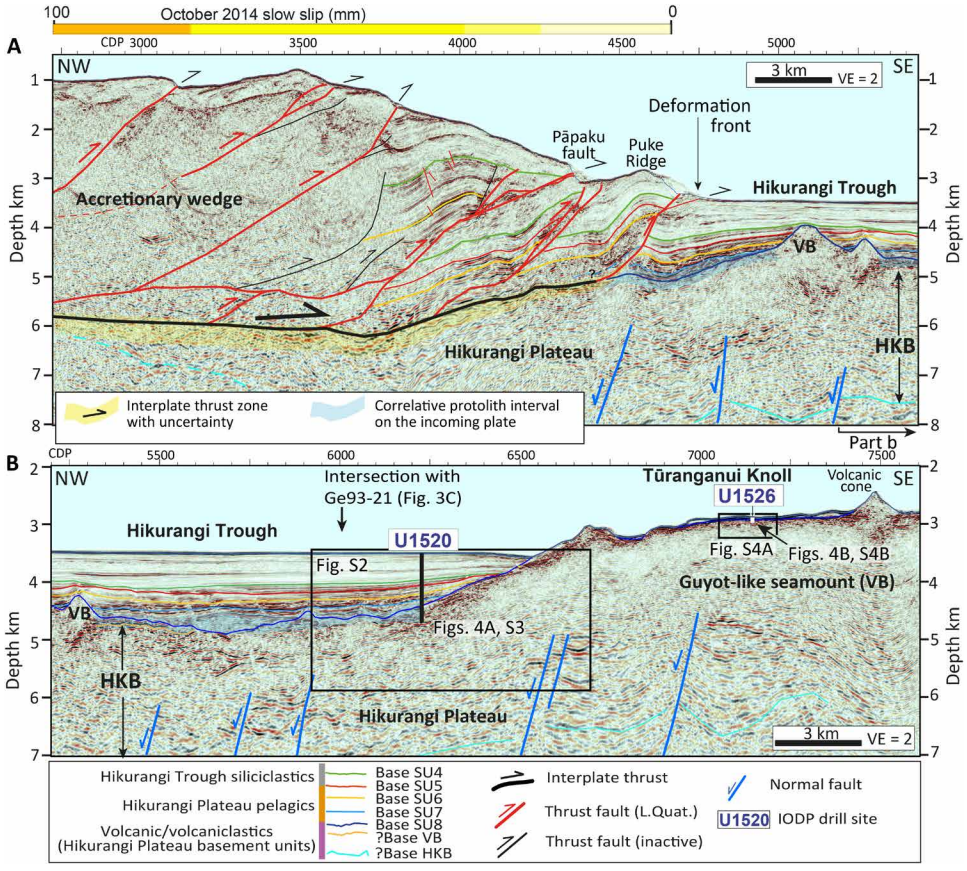


**Fig. 2. Enlarged panels of our interpretations of seismic profile 05CM-04, showing major fault structures, IODP drilling Sites U1520 and U1526, and seismic units (SU) tied to borehole data.** (**A**) Frontal accretionary wedge, major thrust faults (red lines with displacement symbols), megathrust plate interface (bold black line), and normal faults in the subducting plate (blue lines) [modified from (*21*, *25*)]. Yellow shading highlights what we infer to be up to ~500-m uncertainty in the position of the megathrust fault zone. Basement units HKB and VB interpreted here are adapted from (*13*). (**B**) Subduction "inputs" beneath the eastern Hikurangi Trough. Blue shaded zone represents the stratigraphic interval correlated down-dip with the plate interface fault zone. Profile location is shown in Fig. 1. See fig. S1 for uninterpreted sections, and figs. S2 to S4 for integration of core and seismic data.

conglomerate and breccia, and basalt (Lithologic unit II, core photographs 2 to 6; Fig. 4B).

As at Site U1520, physical properties in the volcaniclastic units, as well as the abundance of clay minerals and calcite, are highly variable over short length scales: Porosity ranges from 2 to 44%, and *P*-wave velocity ranges from 1.7 to >5.0 km/s. This variability again reflects the highly heterogeneous texture, composition, alteration, and cementation of the conglomerate. Although some alteration of the basalts and volcaniclastics to smectite and palagonite is also present at Site U1526, they are far less altered than their equivalents at Site U1520.

## DISCUSSION

### Fault zone heterogeneity and implications for slow slip

SSEs are widely thought to be a manifestation of transitional frictional stability. In this model, the fault's frictional behavior lies at the boundary between unstable (velocity-weakening) friction required for stick-slip and stable (velocity-strengthening) behavior that favors aseismic creep (*1*, *3*, *6*). Stress and fluid pressure fluctuations below, within, and above the plate interface are also thought to influence SSEs (*4*, *22*, *26*). It has also recently been suggested that rough crust subduction leads to widespread damage of the overriding plate (*27*, *28*), geometrical complexity of the subduction interface, highly distributed deformation, and stress heterogeneities that would promote aseismic creep and SSEs (*3*, *11*, *18*, *29*).

Our observations from drilling and seismic data indicate that the plate interface in the slow slip source region is likely to be geometrically, compositionally, and rheologically heterogeneous over length scales from centimeters to kilometers. The core and logging data at Sites U1520 and U1526 reveal a highly heterogeneous assemblage of lithologies with widely varying physical properties within the incoming plate interval that correlates down-dip to the plate interface (Figs. 2 and 4). Moreover, a recent full waveform inversion (FWI) of seismic line 05CM-04 demonstrates that the marked variations in Vp observed in the core and borehole data from this interval (Fig. 4) are not limited to centimeter to meter scales, but also vary at larger scales away from the drilling sites as multi-kilometer patches with Vp varying laterally by >1 km/s (*30*). These protoliths to plate interface rocks comprise mainly carbonates and volcaniclastic sediments (widely altered to smectite clay), with minor amounts of siltstone, silty claystone, limestone, and basalt. These carbonate- and volcaniclastic-dominated rocks are not typical of all subduction zones but may be a common feature where seamounts and ridges are subducting (*31*).

The highly variable primary compositions, textures, diagenesis, and alteration of the protolith rocks to the subduction interface

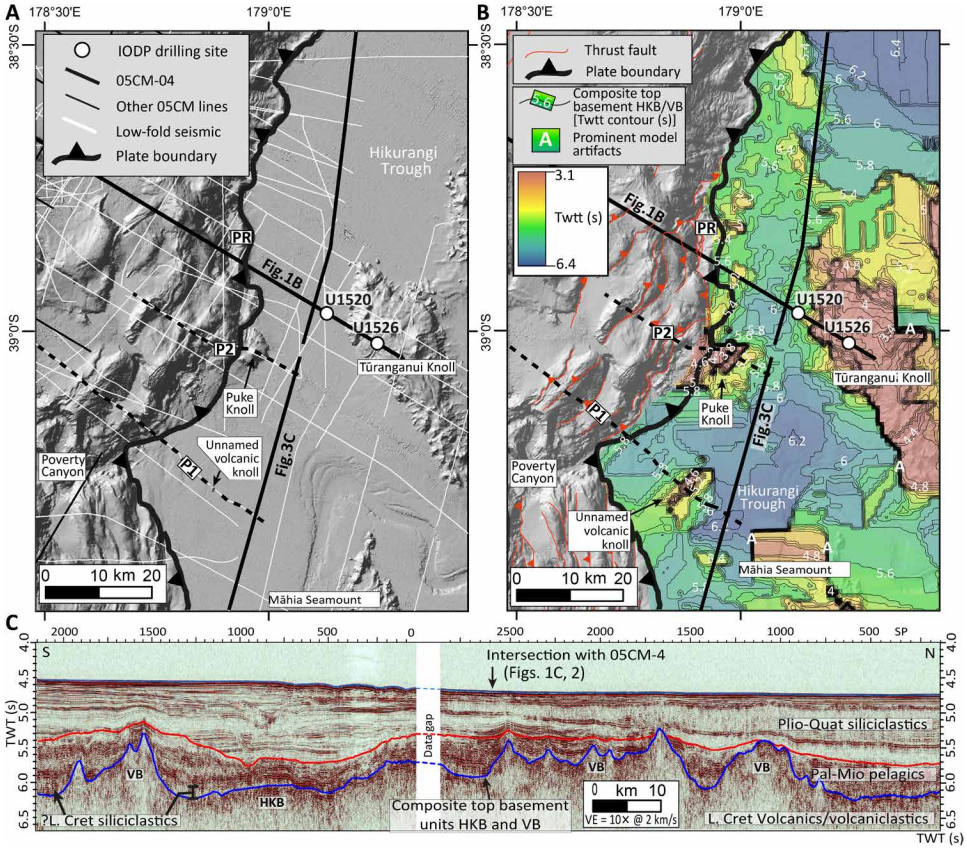


**Fig. 3. Maps of bathymetry, seismic profile coverage, basement surface, and seismic profile along the subducting plate in the region of drilling.** (**A**) Bathymetric hillshade and distribution of seismic profiles used in this study. Black dashed lines with labels P1 and P2 are profiles illustrating basement relief, published in (*17*). PR, Puke Ridge. (**B**) Geometry of the composite top HKB/VB reflection, marking the upper surface of the subducting Hikurangi Plateau basement (derived from our interpretation of the horizon in all seismic profiles shown in part A. Twtt, two-way travel time. (**C**) Contiguous seismic reflection profiles GeoDyNZ Ge93-21a and Ge93-21b highlighting the basement relief and major stratigraphic intervals along the strike of the subducting plate. Profile location is shown in part B. Plio, Pliocene; Quat, Quaternary; Mio, Miocene; Pal, Paleogene; Cret, Cretaceous. Basement units HKB and VB are adapted from (*13*).

assemblage, at scales from centimeters to kilometers, lead to marked variations in cohesion, elastic moduli, strength, and inferred frictional behavior. In particular, compared to relatively weak clay-rich and more highly altered volcaniclastic rocks, the relatively strong carbonates and unaltered to mildly altered basalts can be expected to exhibit very different mechanical properties along the shallow plate interface (*7*, *8*, *32*–*34*).

We also find that the subducting relief of >2 km and roughness at length scales of $10^2$ to $10^4$ m on the top of the composite basement units HKB/VB (Figs. 2 and 3, B and C) has a profound effect on the geometry and host lithologies of the shallow plate interface. Geometric complexity in the fault zone results from the plate interface forming close to the top of the composite basement, the geometry of which is variable (*17*). Furthermore, based on our observations from the seismic profiles and ground truth of the protolith subduction zone stratigraphy from drilling (Fig. 4), the subducting topography controls a wide range of lithological assemblages associated with features on the incoming plate, which ultimately are entrained and brought into contact across the plate interface in different areas (Fig. 5A). This likely leads to a patchy and highly variable suite of plate interface host rocks (Fig. 5B). The nature of lithological mixing and possibly the degree of strain localization will evolve temporally as subduction proceeds and as different rocks are brought into contact with one another. One likely effect of subducting basement relief, coupled with a heterogeneous incoming protolith, is the generation of a geometrically irregular fault zone with variable thickness and strain distribution, and comprising a mosaic of diverse lithologies having markedly different mechanical properties. These spatial variations may also influence the ability of the fault zone to trap, host, and release fluids in association with slip events [e.g., (*22*)].

Our interpretation of geometrical, compositional, and rheological heterogeneity along the plate interface provides an important geological framework for the shallow SSE environment, as well as an explanation for the enigmatic co-existence of patchy (and overlapping) seismic and aseismic slip behavior that is observed from geodetic and seismological data (*18*, *23*, *24*). Some previous field studies, modeling, and laboratory experiments (*2*, *9*–*11*, *33*–*35*) have suggested that heterogeneous fault zones may favor the occurrence of slow slip transients over large earthquake slip. Our inference of highly varied physical properties over a wide range of scales in a known SSE source region, including weak, likely velocity-strengthening smectite-rich volcaniclastics intermingled with stronger, stiffer, and likely velocity-weakening carbonate or unaltered volcanic rocks [e.g., (*32*, *34*)], provides important ground truth for this conceptual model.

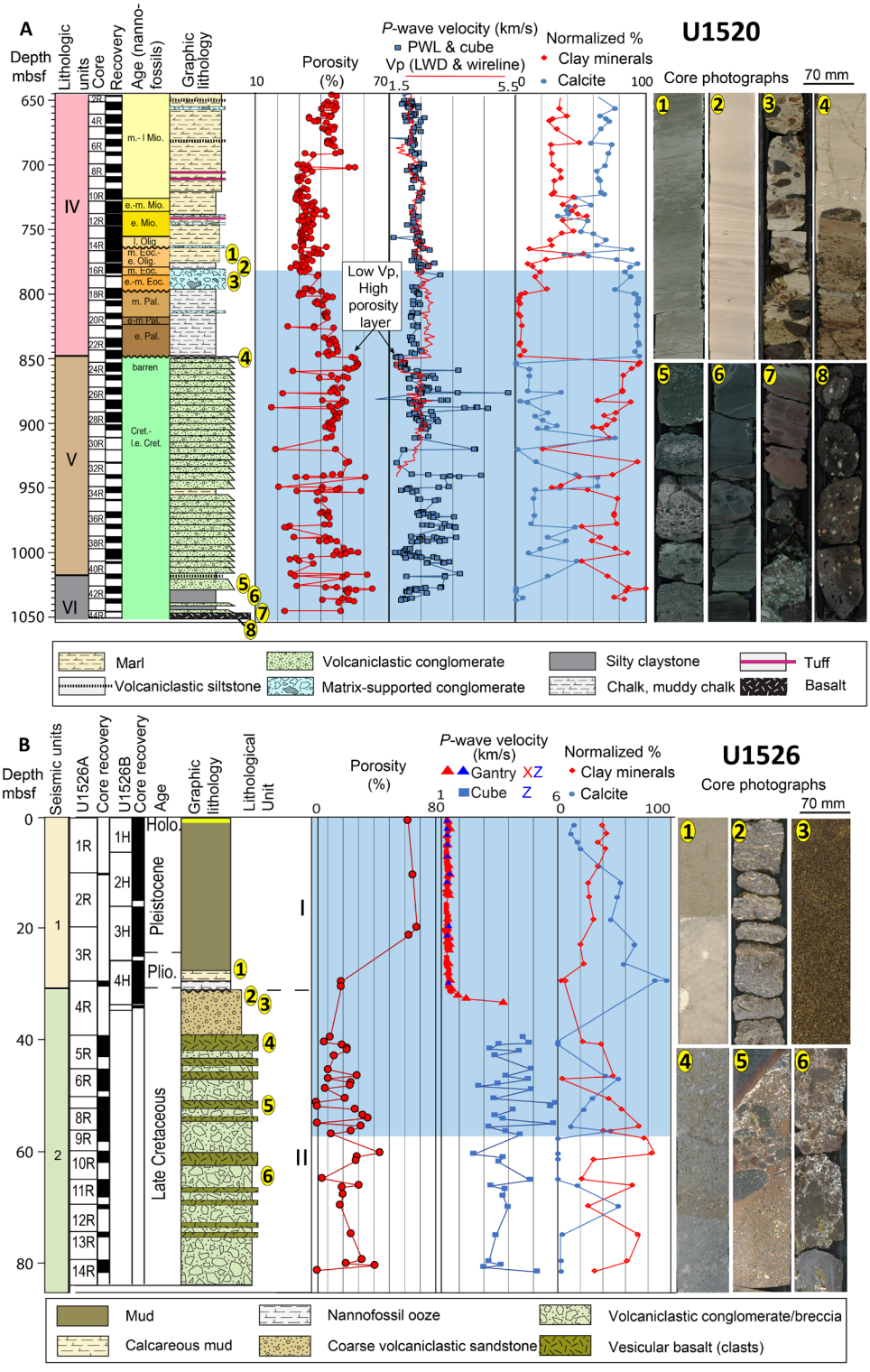


**Fig. 4. IODP core and borehole data from the subducting sequence that is being transported into the plate interface fault zone and SSE source region.** The blue shaded intervals in both panels represent the sequence that correlated to the primary plate interface zone (see Fig. 2). (**A**) Composite of Site U1520, commencing 650 mbsf. White intervals represent no core recovery. Vp, *P*-wave velocity; PWL, *P*-wave logger. Normalized mineral abundances are based on bulk powder x-ray diffraction and coulometric measurements, where total clay minerals + quartz + feldspar + calcite = 100%. Core photographs 1 to 8 (locations noted on the lithology column) include the following: 1, calcareous mudstone; 2, chalk; 3, matrix-supported conglomerate; 4, chalk over volcaniclastic conglomerate; 5, cemented volcaniclastic conglomerate; 6, silty claystone; 7, siltstone over volcaniclastic conglomerate; 8, basalt. (**B**) Composite of Site U1526 data. Core photographs 1 to 6 (locations noted on the lithology column) include the following: 1, calcareous mud over nannofossil ooze; 2, pebble conglomerate over coarse sandstone; 3, coarse volcaniclastic sand; 4, vesicular basalt; 5, pebble-boulder volcaniclastic conglomerate; 6, basalt breccia cemented by calcite.

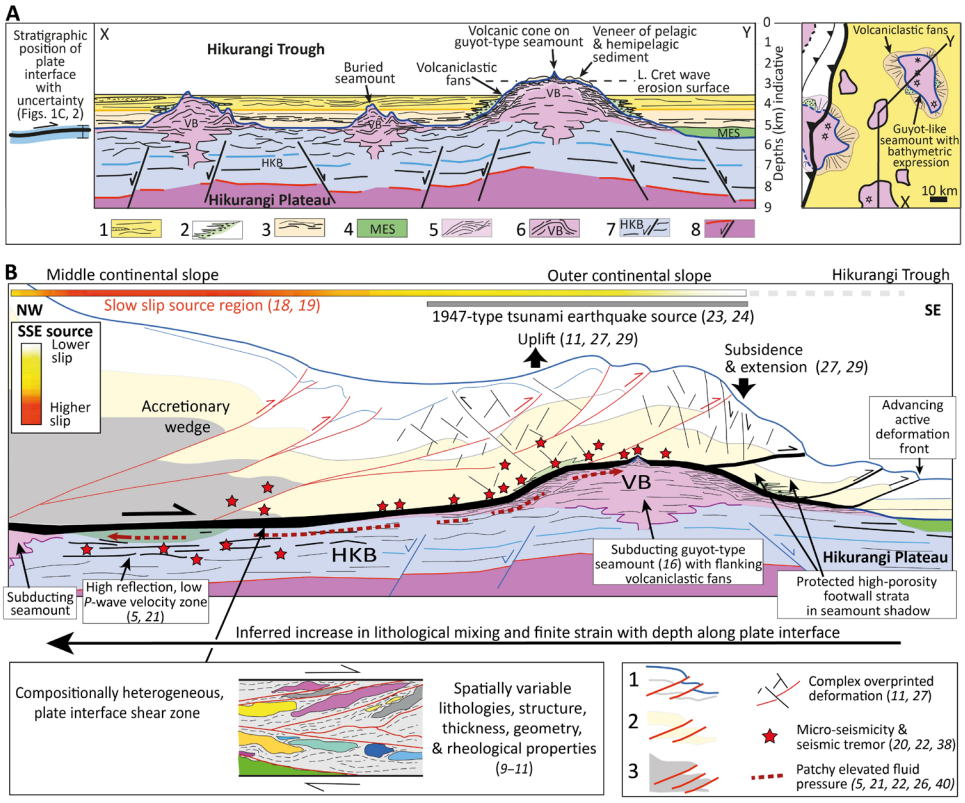


**Fig. 5. Conceptual models of the subducting northern Hikurangi Plateau and adjacent shallow subduction slow slip environment.** (**A**) Generic cross-section X-Y (not to scale) depicting our interpretation of the stratigraphic architecture of the subducting plateau and the position (with uncertainty) where the plate interface forms on subduction of the section. The schematic is derived from seismic data (e.g., Figs. 1B, 2, and 3C) (*17*), drilling results (Fig. 4) (*25*), and crustal and stratigraphic data east of the Hikurangi Trough (*13*, *14*). Legend includes the following: 1, siliciclastic sediments (Site U1520); 2, mass transport deposits (Site U1520); 3, pelagic sediments (chalk, marl, calcareous mudstone, nannofossil ooze) and volcanic tuff (Sites U1520 and U1526); 4, inferred siliciclastics (*13*); 5, volcanic conglomerate/breccia, minor marl, and volcaniclastic sandstones (Sites U1520 and U1526); 6, basaltic volcanics and volcaniclastic sediments (90 to 100 million years old) (U1526) (*13*, *14*); 7, volcaniclastic sediments, siltstone, silty claystone, limestone, and basalt (Site U1520); 8, Hikurangi Plateau basaltic basement (*13*). The right panel is a conceptual map showing the location of section X-Y. Yellow shading, Hikurangi Trough turbidites; pink shading, volcanic seamounts. Small stars atop the broader seamounts are late-stage volcanic cones. (**B**) Generic cross section (not to scale) of the frontal accretionary wedge, depicting the inferred geological framework of the northern Hikurangi shallow slow slip environment. The first-order geometry of the section, adapted from a seismic profile located in the slow slip region 120 km south of the drilling transect (*16*), depicts subduction of a guyot-type seamount of comparable scale to Tūranganui Knoll. The structural, stratigraphic, and seismological elements are derived from our interpretations of seismic data (e.g., Figs. 1B, 2, and 3C), drilling results (Fig. 4) (*25*), and the references labeled. Legend includes the following (*15*–*17*): 1, mainly Pliocene-Quaternary siliciclastic sediments; 2, mainly Paleogene-Miocene pelagic sediments, with possible siliciclastic sequences more landward; 3, imbricated Mesozoic-Paleogene rocks.

We conclude that plate interface heterogeneity at multiple scales is widespread beneath the north Hikurangi margin and that small-scale heterogeneity can affect the behavior of much larger fault patches. Detailed studies of SSEs in both New Zealand and Japan show that slow slip and seismic tremor develop in a similarly irregular and patchy manner, with slip propagating within individual rupture patches at 5 to 10 km/day, and between patches over weeks to months (*10*, *18*). We posit that individual SSE patches (~50- to 100-km scale) comprise a mosaic of smaller heterogeneities from the centimeter to kilometer scale, which link together to produce SSEs over a broader region. This is supported by numerical models that demonstrate that slip events can nucleate and grow from a nucleation patch very much smaller (an order of magnitude or more) than the size of the final slipping patch (*2*, *10*).

Collectively, our direct observations from drilling and seismic reflection data in a region of well-documented SSEs support the idea (to date based largely on modeling studies and conceptual arguments) that shallow slow slip transients can arise from lithological, geometric, and rheological heterogeneity along the plate boundary megathrust. Other subduction zone areas that host shallow slow slip are also characterized by an incoming plate with rough morphology (*3*). On the basis of the results from northern Hikurangi, we expect that globally, this morphology enhances the diversity of lithologies entrained along shallow subduction megathrusts, thus promoting complex slip behavior including slow slip transients.

## MATERIALS AND METHODS

### Seismic reflection data

Profile 05CM-04 was acquired by the New Zealand government in 2005 with a 4140 $m^3$ airgun source array and recorded on a hydrophone streamer consisting of 960 channels and maximum offset of 12 km (*5*, *36*). The shot interval was 37.5 m, and the sampling rate was 2 ms. The two-way travel time migrated section (available from www.nzpam.govt.nz/maps-geoscience/minerals-datapack) was used for core-log-seismic integration (see below). For regional interpretations of seismic stratigraphy, we use a depth conversion of the profile

developed using a high-definition velocity analysis of prestack time migrated data (*21*). The vertical seismic resolution of the section at IODP drilling Sites U1520 and U1526 can be determined as λ/4 [where λ (seismic wavelength) = Vp (*P*-wave velocity)/*f* (dominant frequency)]. At Site U1520, the vertical resolution is about 15 m from ~500 to 700 mbsf, 18 m from 700 to 900 mbsf, and 25 m from 900 to 1200 mbsf. At Site U1526, the vertical resolution is 12 m at 0 to 40 mbsf and 25 m between 40 and 100 mbsf.

Profile 05CM-04 is complemented by other regional seismic data collected across the accretionary wedge and northern Hikurangi Trough by New Zealand and U.S. research institutes (Fig. 3A). These allow us to correlate the critical subduction interface "inputs" sequence along the Hikurangi Trough deformation front for >100 km along strike, spanning our ocean floor drilling transect (Fig. 3, B and C). These sections include low-fold (up to 48 channels) data collected during *R.V. Tangaroa* surveys in 2001, 2011, and 2012 [National Institute of Water and Atmospheric Research, NIWA, voyages TAN0106 (*17*), TAN1114, and TAN1213], *R.V. Rodger Revelle* survey RR1508 in 2015, and *R.V. L'Atalante* on the GeoDyNZ survey in 1993 (*37*). The data collected on surveys TAN1114, TAN1213, and RR1508, specifically in support of IODP Expeditions 372 and 375, were acquired with 300-inch$^3$ Sodera GI gun source and recorded on 48-channel seismic streamers (~825 m length). Processing of these data included binning at 6.25 to 12.5 m CDP spacing, bandpass filtering to 10-35-150-200 Hz, and poststack time migration using a finite difference migration. We created the gridded time surface shown in Fig. 3B from our interpretation of the composite top HKB/VB horizon on all seismic profiles shown in Fig. 3A (and illustrated in Figs. 2 and 3C), using IHS Markit Kingdom software, an ordinary kriging model with 800-m cell size, and spherical variogram.

### Borehole logging data at IODP Sites U1520 and U1526

During IODP Expedition 372 on the *JOIDES Resolution*, we collected a suite of LWD data at Site U1520 from two boreholes about 20 m apart (Hole U1520A at ~CDP 6228 on seismic profile 05CM-04, and Hole U1520B at ~CDP 6227) (*25*). These data include sourceless neutron–gamma ray density (referred to as RHON) between 0 and 750 mbsf measured with the NeoScope tool, and *P*-wave velocity logs between 0 and 721 mbsf produced from the SonicScope tool. Data sampling for both density and *P*-wave velocity is 0.1524 m. The waveform data were processed by Schlumberger in Perth. We acquired overlapping wireline downhole logging sonic and gamma ray data up to 944 mbsf in an adjacent Hole U1520C (at ~CDP 6226 on seismic profile 05CM-04) during IODP Expedition 375 (*25*).

### Drill core data at IODP Sites U1520 and U1526

We use lithological, biostratigraphic, and physical properties data from drill cores collected during IODP Expedition 375 on the *JOIDES Resolution* (*25*). Cores were acquired with the Rotary Core Barrel (RCB) at Holes U1520C (located at CDP 6226 on profile 05CM-04) and U1526A (~CDP 7144), and with the Advanced Piston Corer (APC) at Hole U1526B. The laboratory physical properties were measured following standard methods used in recent IODP expeditions (*25*). Visual descriptions of the lithology, sedimentary features, and structure were based on observations of the archive half of the split core. Normalized mineral abundances were determined from bulk powder x-ray diffraction and coulometric measurements, where total clay minerals + quartz + feldspar + calcite = 100%. Biostratigraphic ages were derived from foraminifers and nannofossils.

### Integration of core, logging, and seismic data

A seismic-well tie was developed at each of Sites U1520 and U1526 to correlate physical property changes in geophysical logging, lithology, and core physical properties data with seismic reflections and facies on profile 05CM-04 to extrapolate results away from the drilling sites. Synthetic seismograms were developed in three steps involving (i) production of a reflection coefficient model from logging and/or core velocity and density measurements, (ii) calculation of vertical reflection times from logging data and core measurements, and (iii) convolution of the reflection coefficient model with a source wavelet.

At Site U1520, we developed a time-depth relationship by splicing the *P*-wave velocity (Vp) data acquired by the LWD SonicScope tool with overlapping wireline downhole logging sonic data to produce a continuous sonic log from 0 to 944 mbsf. The combined Vp log was then smoothed over a 3-m window to produce a profile relevant for the vertical resolution of the seismic data. The model at Site U1520 compares reasonably well with velocity depth relationships from prestack depth migration (PSDM) and FWI of line 05CM-04 (*21*, *30*). To develop a synthetic seismogram, we used the LWD sourceless neutron–gamma ray density (RHON) from the NeoScope tool from 0 to 750 mbsf (from Holes U1520A and U1520B) and integrated that with a density log for the interval 750 to 944 mbsf constructed from bulk density measurements from cores at Hole U1520C. The combined density log was then also smoothed over a 3-m window.

We extracted a preferred source wavelet from profile 05CM-04 by stacking 10 adjacent seismic traces from a flat region at Site U1520 to yield a high signal-to-noise ratio. This wavelet was convolved with the reflection coefficient log measured in two-way travel time to produce a synthetic seismic trace that can be compared with seismic profile 05CM-04 in the vicinity of CDP 6227. The wavelets were convolved with a reflectivity series R expressed as the following

$$R = (\mathrm{Vp}_2\rho_2 - \mathrm{Vp}_1\rho_1)/(\mathrm{Vp}_1\rho_1 + \mathrm{Vp}_2\rho_2)$$

where $\mathrm{Vp}_1$ and $\mathrm{Vp}_2$ and $\rho_1$ and $\rho_2$ are the acoustic velocity and density in the upper layer and lower layers, respectively. The close match between the synthetic trace and profile 05CM-04 provides high confidence in the correlation between the LWD, wireline, core, and seismic reflection data.

At Site U1526, where no LWD or wireline downhole logging data were acquired during drilling, we built a simplified lithological model and populated it with velocity and density data from laboratory measurements from core samples from Holes U1526A and U1526B to create a synthetic seismic trace. The model consisted of 30 m of pelagic sediment with Vp of 1510 m/s, overlying a volcaniclastic conglomerate and breccia sequence between 30 and 84 mbsf with a mean Vp of 3805 m/s. The latter mean velocity is considerably higher than stacking velocities and predictions made by PSDM (*21*). Although more complicated models are possible, we consider that the synthetic seismic trace derived from the velocity model, discrete core sample density data, and an appropriate source wavelet matches adequately the real seismic data on 05CM-04. Notably, the model reproduces the high-amplitude reflection at the observed contact between the pelagic cover sequence and the underlying volcaniclastics.

## SUPPLEMENTARY MATERIALS

Supplementary material for this article is available at http://advances.sciencemag.org/cgi/content/full/6/13/eaay3314/DC1

Members of IODP Expedition 372 Scientists
Fig. S1. Uninterpreted panels of seismic line 05CM-04.
Fig. S2. Seismic reflection profile across the eastern side of the Hikurangi Trough and buried lower flank of Tūranganui Knoll seamount in the vicinity of IODP Site U1520.
Fig. S3. Lithological log of the lower "subduction inputs" section of IODP Site U1520, below 650 mbsf, tied to seismic reflection profile 05CM-04.
Fig. S4. Enlarged seismic section of the crest of Tūranganui Knoll seamount, in the vicinity of IODP Site U1526, and lithological log tied to the seismic data.

## REFERENCES AND NOTES


1. Y. Liu, J. R. Rice, Spontaneous and triggered aseismic deformation transients in a subduction fault model. *J. Geophys. Res.* **112**, (2007).
2. R. M. Skarbek, A. W. Rempel, D. A. Schmidt, Geologic heterogeneity can produce aseismic slip transients. *Geophys. Res. Lett.* **39**, (2012).
3. D. M. Saffer, L. M. Wallace, The frictional, hydrologic, metamorphic and thermal habitat of shallow slow earthquakes. *Nat. Geosci.* **8**, 594–600 (2015).
4. S. Kodaira, T. Iidaka, A. Kato, J.-O. Park, T. Iwasaki, Y. Kaneda, High pore fluid pressure may cause silent slip in the Nankai trough. *Science* **304**, 1295–1298 (2004).
5. R. Bell, R. Sutherland, D. H. N. Barker, S. Henrys, S. Bannister, L. M. Wallace, J. Beavan, Seismic reflection character of the Hikurangi subduction interface, New Zealand, in the region of repeated Gisborne slow slip events. *Geophys. J. Int.* **180**, 34–48 (2010).
6. J. R. Leeman, D. M. Saffer, M. M. Scuderi, C. Marone, Laboratory observations of slow earthquakes and the spectrum of tectonic fault slip modes. *Nat. Commun.* **7**, 11104 (2016).
7. H. S. Rabinowitz, H. M. Savage, R. M. Skarbek, M. J. Ikari, B. M. Carpenter, C. Collettini, Frictional behavior of input sediments to the Hikurangi Trench, New Zealand. *Geochem. Geophys. Geosyst.* **19**, 2973–2990 (2018).
8. R. M. Kurzawski, A. R. Niemeijer, M. Stipp, D. Charpentier, J. H. Behrmann, C. J. Spiers, Frictional properties of subduction input sediments at an erosive convergent continental margin and related controls on décollement slip modes: The costa rica seismogenesis project. *J. Geophys. Res. Solid Earth* **123**, 8385–8408 (2018).
9. Å. Fagereng, R. Sibson, Mélange rheology and seismic style. *Geology* **38**, 751–754 (2010).
10. R. Ando, N. Takeda, T. Yamashita, Propagation dynamics of seismic and aseismic slip governed by fault heterogeneity and Newtonian rheology. *J. Geophys. Res.* **117**, (2012).
11. K. Wang, S. L. Bilek, Invited review paper: Fault creep caused by subduction of rough seafloor relief. *Tectonophysics* **610**, 1–24 (2014).
12. L. M. Wallace, J. Beavan, R. McCaffrey, D. Darby, Subduction zone coupling and tectonic block rotations in the North Island, New Zealand. *J. Geophys. Res.* **109**, B12406 (2004).
13. B. Davy, K. Hoernle, R. Werner, Hikurangi Plateau: Crustal structure, rifted formation, and Gondwana subduction history. *Geochem. Geophys. Geosyst.* **9**, Q07004 (2008).
14. K. Hoernle, F. Hauff, P. van den Bogaard, R. Werner, N. Mortimer, J. Geldmacher, D. Garbe-Schöenberg, B. Davy, Age and geochemistry of volcanic rocks from the Hikurangi and Manihiki oceanic Plateaus. *Geochim. Cosmochim. Acta* **74**, 7196–7219 (2010).
15. J.-Y. Collot, K. Lewis, G. Lamarche, S. Lallemand, The giant Ruatoria debris avalanche on the northern Hikurangi margin, New Zealand; result of oblique seamount subduction. *J. Geophys. Res.* **106** (B9), 19271–19297 (2001).
16. P. M. Barnes, G. Lamarche, J. Bialas, I. Pecher, S. Henrys, G. Netzeband, J. Greinert, J. J. Mountjoy, K. Pedley, G. Crutchley, Tectonic and geological framework for gas hydrates and cold Seeps on the Hikurangi subduction margin, New Zealand. *Mar. Geol.* **272**, 26–48 (2010).
17. K. L. Pedley, P. M. Barnes, J. R. Pettinga, K. B. Lewis, Seafloor structural geomorphic evolution of the accretionary frontal wedge in response to seamount subduction, Poverty Indentation, New Zealand. *Mar. Geol.* **270**, 119–138 (2010).
18. L. M. Wallace, J. Beavan, S. Bannister, C. Williams, Simultaneous long-term and short-term slow slip events at the Hikurangi subduction margin, New Zealand: Implications for processes that control slow slip event occurrence, duration, and migration. *J. Geophys. Res.* **117**, B11402 (2012).
19. L. M. Wallace, S. C. Webb, Y. Ito, K. Mochizuki, R. Hino, S. A. Henrys, S. Y. Schwartz, A. F. Sheehan, Slow slip near the trench at the Hikurangi subduction zone, New Zealand. *Science* **352**, 701–704 (2016).
20. E. K. Todd, S. Y. Schwartz, C. Williams, A. F. Sheehan, K. Mochizuki, S. Henrys, Y. Ito, L. M. Wallace, S. Webb, Earthquakes and tremor linked to seamount subduction during shallow slow slip at the Hikurangi margin, New Zealand. *J. Geophys. Res.* **123**, 6769–6783 (2018).
21. D. H. N. Barker, S. Henrys, F. C. Tontini, P. M. Barnes, D. Bassett, E. Todd, L. M. Wallace, Geophysical constraints on the relationship between seamount subduction, slow slip and tremor and the north Hikurangi subduction zone, New Zealand. *Geophys. Res. Lett.* **45**, 12804–12813 (2018).
22. E. Warren-Smith, B. Fry, L. Wallace, E. Chon, S. Henrys, A. Sheehan, K. Mochizuki, S. Schwartz, S. Webb, S. Lebedev, Episodic stress and fluid pressure cycling in subducting oceanic crust during slow slip. *Nat. Geosci.* **12**, 475–481 (2019).
23. D. I. Doser, T. H. Webb, Source parameters of large historical (1917 – 1961) earthquakes, North Island, New Zealand. *Geophys. J. Int.* **152**, 795–832 (2003).
24. R. Bell, C. Holden, W. Power, X. Wang, G. Downes, Hikurangi margin tsunami earthquake generated by slow seismic rupture over a subducted seamount. *Earth Planet. Sci. Lett.* **397**, 1–9 (2014).
25. L. M. Wallace, D. M. Saffer, P. M. Barnes, I. A. Pecher, K. E. Petronotis, L. J. LeVay, Expedition 372/375 Scientists, Hikurangi subduction margin coring, logging, and observatories, in *Proceedings of the International Ocean Discovery Program* (International Ocean Discovery Program, 2019).
26. S. Ellis, Å. Fagereng, D. Barker, S. Henrys, D. Saffer, L. Wallace, C. Williams, R. Harris, Fluid budgets along the northern Hikurangi subduction margin, New Zealand: The effect of a subducting seamount on fluid pressure. *Geophys. J. Int.* **202**, 277–297 (2015).
27. S. Dominguez, J. Malavieille, S. E. Lallemand, Deformation of accretionary wedges in response to seamount subduction: Insights from sandbox experiments. *Tectonics* **19**, 182–196 (2000).
28. R. von Huene, When seamounts subduct. *Science* **321**, 1165–1166 (2008).
29. J. B. Ruh, V. Sallarès, C. R. Ranero, T. Gerya, Crustal deformation dynamics and stress evolution during seamount subduction: High-resolution 3-D numerical modeling. *J. Geophys. Res. Solid Earth* **121**, 6880–6902 (2016).
30. M. Gray, R. Bell, J. Morgan, S. Henrys, D. Barker; The IODP Expedition 372 and 375 science parties, Imaging the shallow subsurface structure of the Hikurangi subduction zone, New Zealand, using Full-Waveform Inversion. *J. Geophys. Res. Solid Earth* **124**, 9049–9074 (2019).
31. T. Plank, The chemical composition of subducting sediments. *Treatise Geochem.* **4**, 607–629 (2014).
32. M. J. Ikari, C. Marone, D. M. Saffer, A. J. Kopf, Slip weakening as a mechanism for slow earthquakes. *Nat. Geosci.* **6**, 468–472 (2013).
33. C. Boulton, A. R. Niemeijer, C. J. Hollis, J. Townend, M. D. Raven, D. K. Kulhanek, C. L. Shepherd, Temperature-dependent frictional properties of heterogeneous Hikurangi Subduction Zone input sediments, ODP Site 1124. *Tectonophysics* **757**, 123–139 (2019).
34. T. Tesei, C. Collettini, M. R. Barchi, B. M. Carpenter, G. Di Stefano, Heterogeneous strength and fault zone complexity of carbonate-bearing thrusts with possible implications for seismicity. *Earth Planet. Sci. Lett.* **408**, 307–318 (2014).
35. S. Webber, S. Ellis, Å. Fagereng, Virtual shear box experiments of stress and slip cycling within a subduction interface mélange. *Earth Planet. Sci. Lett.* **488**, 27–35 (2018).
36. Multiwave, *05CM 2D Seismic Survey, Offshore East Coast—North Island* (Ministry of Economic Development, 2005), 280 pp.
37. J.-Y. Collot, J. Delteil, K. Lewis, B. Davy, G. Lamarche, J.-C. Audru, P. M. Barnes, F. Chanier, E. Chaumillon, S. Lallemand, B. Mercier de Lepinay, A. Orpin, B. Pelletier, M. Sosson, B. Toussaint, C. Uruski, From oblique subduction to intra-continental transpression: Structures of the southern Kermadec-Hikurangi margin from multibeam bathymetry, side-scan sonar and seismic reflection. *Mar. Geophys. Res.* **18**, 357–381 (1996).
38. E. K. Todd, S. Y. Schwartz, Tectonic tremor along the northern Hikurangi Margin, New Zealand, between 2010 and 2015. *J. Geophys. Res. Solid Earth* **121**, 8706–8719 (2016).
39. C. A. Williams, D. Eberhart-Phillips, S. Bannister, D. H. N. Barker, S. Henrys, M. Reyners, R. Sutherland, Revised interface geometry for the Hikurangi subduction zone, New Zealand. *Seismol. Res. Lett.* **84**, 1066–1073 (2013).
40. D. Bassett, R. Sutherland, S. Henrys, Slow wavespeeds and fluid overpressure in a region of shallow geodetic locking and slow slip, Hikurangi subduction margin, New Zealand. *Earth Planet. Sci. Lett.* **389**, 1–13 (2014).


**Acknowledgments:** This research used samples and data provided by the IODP. We thank all staff onboard the *JOIDES Resolution* during Expeditions 372 and 375 for their support. We acknowledge all staff onboard the *Tangaroa* and R. Revelle for assistance with seismic data acquisition on surveys TAN1114, TAN1213, and RR1508. We thank S. Woelz and D. Bassett for assistance with seismic data pre-expedition. The manuscript benefitted greatly from constructive reviews provided by K. Wang and an anonymous reviewer. **Funding:** P.M.B., L.M.W., S.He., and D.H.N.B. acknowledge support from the Endeavour fund, administered by New Zealand's Ministry for Business, Innovation, and Employment Contract CO5X1605, as well as NIWA SSIF core funding. R.E.B. received funding from NERC IODP Moratorium Grant NE/S00291X/1. A.F. received funding from NERC IODP Moratorium Grant NE/S002731/1 and ERC Starting Grant 715836 "MICA." S.K. acknowledges funding from the German Research Foundation (grant KU2685/11-1). C.H.E.d.O. thanks CAPES/IODP Fellowship (88881.131465/2016-01). A.D.W. was supported by IODP UK grant NE/S008853/1. K.E.P. and L.J.L. received funding from the IODP JRSO (NSF grant 1326927). All other U.S. authors were supported by the U.S. Science Support Program. D.G. thanks the Sêr Cymru NRN-LCEE and NERC UKIODP grant NE/R016992/1 for funding and travel support. A.G. was supported by KETEP MOTIE (no. 20168510030830). A.H. received funding from Deutsche Forschungsgemeinschaft Grant HU-1789/5-1. G.Y.K. and H.L. thank K-IODP for support. X.L. was supported by IODP-China, 20180305, Tongji University. F.M. thanks IODP Italia-ECORD. D.D.M. and A.Ge. thank the Geological Survey Ireland. K.U.H. thanks IODP

Germany. X.W. was supported by National Natural Science Foundation of China (41976077). M.B.C., P.M.B., L.M.W., M.P.C., and C.L.S. were supported by the Australia/NZ IODP Consortium (ANZIC). **Author contributions:** P.M.B. coauthored IODP proposal 781A, led the acquisition and interpretation of pre-drilling seismic and bathymetric data (survey TAN1114), co-led IODP drilling Expedition 372 that collected the LWD data, and co-led the conception and writing of the paper. L.M.W. and D.M.S. co-led IODP proposal 781A, co-led IODP drilling Expedition 375 that collected the core and wireline data, and co-led conception and writing of the paper. M.B.U. contributed to proposal development and operational planning of the expeditions. R.E.B., M.B.U., A.F., F.M., H.M.S., H.S.R., J.K.M., E.J.S., A.E.C., D.D.M., L.J.L., K.E.P., M.J.I., H.Ki., G.F.M., and S.M.B. provided key input in the writing of the paper. I.A.P. co-led IODP Expedition 372 that collected the LWD data. K.E.P. and L.J.L. were the Expedition Project Managers for IODP drilling Expeditions 375 and 372, respectively. S.He. contributed to IODP proposal 781A; led the processing of seismic reflection data from surveys TAN1114, TAN1213, and RR1508; and co-led the interpretation and compilation of predrilling site data. S.He. and D.H.N.B. processed and provided the depth converted seismic section, which was used to locate the drilling targets and is illustrated in the paper. J.J.M. (Expedition 372) contributed to IODP proposal 781A, and the acquisition and compilation of seismic and bathymetric data (surveys TAN1114 and TAN1213). The remaining authors contributed to critical shipboard analysis on Expeditions 372 and 375. The IODP Expedition 372 science participants contributed to the acquisition of the LWD data. **Competing interests:** The authors declare that they have no competing interests. **Data and materials availability:** All IODP drilling data are available from IODP at http://iodp.tamu.edu/scienceops/expeditions/hikurangi_subduction_margin.html. The original seismic reflection section 05CM-04 is available from New Zealand Petroleum and Minerals at https://www.nzpam.govt.nz/. The depth seismic section used in this paper is available upon request from S.He. and D.H.N.B. Bathymetry data are available upon request from the senior author.

Submitted 9 June 2019
Accepted 2 January 2020
Published 25 March 2020
10.1126/sciadv.aay3314

**Citation:** P. M. Barnes, L. M. Wallace, D. M. Saffer, R. E. Bell, M. B. Underwood, A. Fagereng, F. Meneghini, H. M. Savage, H. S. Rabinowitz, J. K. Morgan, H. Kitajima, S. Kutterolf, Y. Hashimoto, C. H. Engelmann de Oliveira, A. Noda, M. P. Crundwell, C. L. Shepherd, A. D. Woodhouse, R. N. Harris, M. Wang, S. Henrys, D. H. Barker, K. E. Petronotis, S. M. Bourlange, M. B. Clennell, A. E. Cook, B. E. Dugan, J. Elger, P. M. Fulton, D. Gamboa, A. Greve, S. Han, A. Hüpers, M. J. Ikari, Y. Ito, G. Y. Kim, H. Koge, H. Lee, X. Li, M. Luo, P. R. Malie, G. F. Moore, J. J. Mountjoy, D. D. McNamara, M. Paganoni, E. J. Screaton, U. Shankar, S. Shreedharan, E. A. Solomon, X. Wang, H.-Y. Wu, I. A. Pecher, L. J. LeVay, IODP Expedition 372 Scientists, Slow slip source characterized by lithological and geometric heterogeneity. *Sci. Adv.* **6**, eaay3314 (2020).